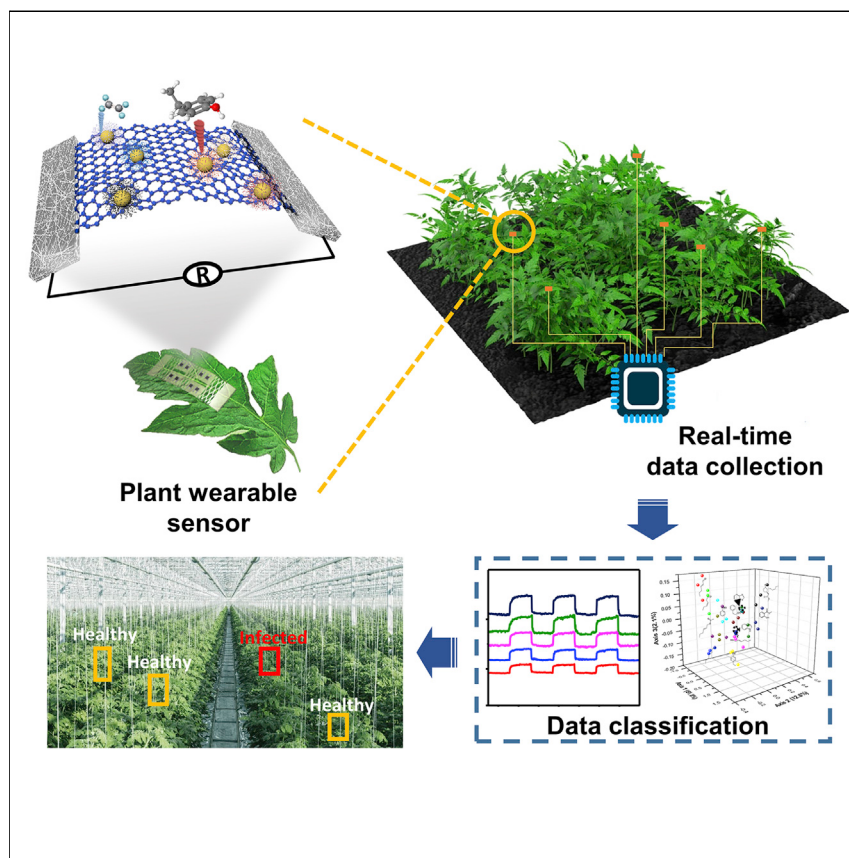


Article

Real-time monitoring of plant stresses via chemiresistive profiling of leaf volatiles by a wearable sensor



We demonstrate a wearable sensor platform for real-time profiling of plant volatile organic compound markers based on a chemiresistive sensor array made of reduced graphene oxide functionalized with various ligands. This multiplexed sensor array allows for accurate classification of 13 individual plant volatiles with >97% classification accuracy, and detection of late blight infection and mechanical damage noninvasively. This lightweight gas sensor platform could be a powerful alternative to other diagnostics tools available for long-term monitoring of plant health in the field.

Demonstrate

Proof-of-concept of performance with intended application/response

4

Zheng Li, Yuxuan Liu, Oindrila Hossain, ..., Jean B. Ristaino, Yong Zhu, Qingshan Wei

yzhu7@ncsu.edu (Y.Z.)
qwei3@ncsu.edu (Q.W.)

Highlights

We report a leaf-attachable VOC sensor for real-time profiling of plant volatiles

The sensor patch detects plant VOCs at low-ppm concentrations

13 individual plant VOCs were differentiated with >97% accuracy by the sensor

It has been used to detect tomato late blight and mechanical damage noninvasively



Article

Real-time monitoring of plant stresses via chemiresistive profiling of leaf volatiles by a wearable sensor

Zheng Li,^{1,2,7} Yuxuan Liu,^{3,7} Oindrila Hossain,¹ Rajesh Paul,¹ Shanshan Yao,^{3,4} Shuang Wu,³ Jean B. Ristaino,^{5,6} Yong Zhu,^{3,*} and Qingshan Wei^{1,6,8,*}

SUMMARY

Determination of plant stresses such as infections by plant pathogens is currently dependent on time-consuming and complicated analytical technologies. Here, we report a leaf-attachable chemiresistive sensor array for real-time fingerprinting of volatile organic compounds (VOCs) that permits noninvasive and early diagnosis of plant diseases, such as late blight caused by *Phytophthora infestans*. The imperceptible sensor patch integrates an array of graphene-based sensing materials and flexible silver nanowire electrodes on a kirigami-inspired stretchable substrate, which can minimize strain interference. The sensor patch has been mounted on live tomato plants to profile key plant volatiles at low-ppm concentrations with fast response (<20 s). The multiplexed sensor array allows for accurate detection and classification of 13 individual plant volatiles with >97% classification accuracy. The wearable sensor patch was used to diagnose tomato late blight as early as 4 days post inoculation and abiotic stresses such as mechanical damage within 1 h.

INTRODUCTION

Phytophthora infestans is the causal agent of late blight and one of the most destructive diseases of economically important crops such as tomato and potato.¹ Due to the rapid rate of spread, late blight poses a significant threat to global food chain security. It is estimated that global crop losses caused by late blight and the cost to control it exceed US \$6.7 million annually.² Therefore, early diagnosis and intervention to control late blight is essential for effective prevention and management of this infectious plant pathogen.³

Conventional approaches for plant pathogen detection include a wide range of biomolecular assays, including PCR,^{4–6} ELISA,^{7,8} and lateral flow immunostrips.⁹ Loop-mediated isothermal amplification,^{10,11} on the other hand, is more rapid and applicable for field assays but generally requires destructive sample preparation.^{7,8} Overall, these methods either suffer from cumbersome assay protocols or are limited by the detection sensitivity and specificity when performed in the field.^{12–14} In recent years, rapid profiling of characteristic volatile organic compounds (VOCs) has attracted tremendous attention as a promising noninvasive technique for early diagnosis of plant diseases. Studies have revealed that VOCs emitted by plant tissues are closely associated with the metabolic or pathologic processes in the live plant system and reflect the physiological state of the individual plant.^{15,16} It has been reported that an elevated level of C6-aldehydes (e.g., (E)-2-hexenal,

Progress and potential

Developing a noninvasive sensing technique that enables continuous plant volatile organic compound (VOC) analysis in their natural habitat is essential to capture the VOC flux from plants for accurate monitoring of plant diseases and stresses. Several wearable sensor platforms have recently been developed that can be attached to living plants for continuous monitoring. However, detecting and discrimination of plant chemical cues such as VOCs have rarely been reported by using a wearable sensor platform. Here, a real-time VOC-profiling sensor device on a stretchable substrate has been developed for instant monitoring of plant host responses for early disease diagnosis and rapid stress identification of living plants.



(*E*)-2-hexanal, and (*Z*)-3-hexenal), terpenes (e.g., terpinene, sabinene, and ocimene), alcohols (e.g., linalool), and terpineol were observed from the headspace gas of injured or infected tomato leaves or stems,^{17–19} which makes the VOC profiles of healthy and unhealthy plants differentiable from each other and become appealing diagnostic markers. In particular, the emission level of (*E*)-2-hexenal rises extremely high (4- to 6-fold versus the healthy control) for tomato leaves when infected with *P. infestans*.¹⁹ However, the chemical composition of the VOC mixture released by plant tissues (e.g., leaves, stems, roots) is complex and varies over time, which poses great challenges in accurate recognition and quantification of different VOC species in the gas mixture. In addition, it is widely accepted that there is no single VOC that is attributed to a specific disease or stress condition. For diagnostic applications, collective analysis of a panel of plant VOCs is needed to generate a molecular “fingerprint” profile for reliable detection of plant diseases and stresses.^{20–22} In this regard, a few laboratory techniques such as gas chromatography-mass spectrometry (GC-MS)^{23–25} have emerged as an effective way to analyze gaseous biomarkers with high sensitivity and specificity. However, GC-based methods require time-consuming sample analysis and complicated instrument operation, which restrict their uses to centralized laboratories.²⁶

An alternative method of analyzing complicated gas mixture is to use array-based sensors, such as electronic (e-noses),^{27–29} optoelectronic, and chemical noses.^{30–33} All of these techniques comprise an array of cross-reactive sensors that mimics the function of olfactory receptors in mammalian noses. The sensor array generates a distinctive pattern of electronic, optical, or chemical signals upon exposure to VOCs for the accurate classification of both single and mixed VOCs.³² We have recently reported a smartphone-based colorimetric sensing array using a series of plasmonic nanoparticles or chemoresponsive dyes for the detection and discrimination of specific VOC biomarkers generated from *P. infestans*-infected tomato leaves, and diagnosis of late blight in tomato with >95% accuracy using both laboratory-inoculated or field-collected leaf samples.³⁴ The array-based test strip can distinguish VOCs over a broad range of organic compounds, including aliphatic or aromatic aldehydes or ketones, alcohols, esters, and carboxylic acids. However, the disposable sensor array strip equipped with a handheld smartphone scanner has disadvantages in field applications, such as lack of the capability to perform long-term and real-time monitoring of plant symptoms. To this end, developing a continuous and noninvasive sensing technique that can perform comprehensive analysis of plant VOC emissions in their natural habitat will be essential to capture the true VOC flux for more accurate monitoring of both biotic and abiotic plant stresses.

Significant progress has been made in flexible and stretchable electronics in the past decade.^{35–40} Several wearable sensor platforms have been developed that can be attached to living plants for continuous monitoring of plant health, such as the growth,^{41–44} microclimate (e.g., humidity, temperature, and light),^{45–48} drought stress or transpiration,^{49–51} and pesticide application.⁵² However, existing plant-wearable sensor platforms have so far only been demonstrated for the detection of mechanical (e.g., growth, stretching, strain) or environmental (e.g., temperature, light) parameters. On the other hand, detection and discrimination of chemical or biological signals has not been fully explored by using a plant-wearable sensor. Lee et al. reported a carbon nanotube-based wearable field-effect transistor device for gas sensing on the surface of plant leaves.⁵³ However, only simulant gas molecules such as dimethyl methylphosphonate but no actual plant VOCs has been analyzed using the wearable sensor. As such, a wearable sensor platform that can

¹Department of Chemical and Biomolecular Engineering, North Carolina State University, Raleigh, NC 27695, USA

²Institute for Advanced Study, Shenzhen University, Shenzhen 518060, China

³Department of Mechanical and Aerospace Engineering, North Carolina State University, Raleigh, NC 27695, USA

⁴Department of Mechanical Engineering, Stony Brook University, Stony Brook, NY 11794-2300, USA

⁵Department of Entomology and Plant Pathology, Raleigh, NC 27695, USA

⁶Emerging Plant Disease and Global Food Security Cluster, North Carolina State University, Raleigh, NC 27695, USA

⁷These authors contributed equally

⁸Lead contact

*Correspondence: yzhu7@ncsu.edu (Y.Z.), qwei3@ncsu.edu (Q.W.)

<https://doi.org/10.1016/j.matt.2021.06.009>

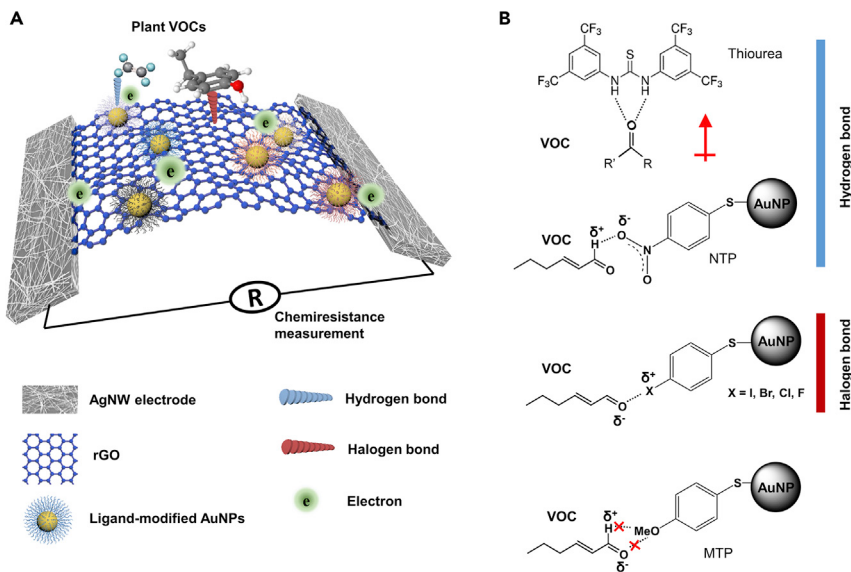


Figure 1. Sensing mechanism of graphene-based sensors

(A) Schematic diagram of the wearable sensor with graphene-based sensing materials and soft AgNW electrodes.

(B) Proposed mechanism showing hydrogen- or halogen-bonding interactions between plant VOCs and employed chemical ligands.

measure VOC emissions from plants in real time is urgently needed to ensure the early detection of plant diseases or stresses.

In this work, we demonstrate a wearable sensor platform for real-time profiling of plant VOC markers based on a chemiresistive sensor array made of reduced graphene oxide (rGO) functionalized with various ligands (Figure 1). This multiplexed sensor array includes two different types of rGO sensors that can form reversible interactions with various plant VOCs via either hydrogen or halogen bonding. The rGO nanosheets are modified either with functionalized gold nanoparticles (AuNPs) or directly with chemical ligands containing different recognition groups (Figure S1B) to selectively capture oxygen- or nitrogen-containing organic compounds (e.g., aldehydes, ketones, alcohols) from a wide variety of plant VOCs (Figure S1A).^{26,54,55} The optimized sensor array composed of 4–8 rGO sensors exhibits excellent discrimination results among different individual plant VOCs, such as green leaf volatiles (GLVs) and phytohormones under ambient conditions. The sensor patch was insensitive to common mechanical perturbations such as wind blowing and hand touching as a result of the stretchable kirigami-based substrate. The environmental perturbations from temperature and humidity were also investigated. Using this sensor platform, early detection of *P. infestans* infection (within 4 days of inoculation) and abiotic stresses such as mechanical injury on different parts of tomato plants were achieved by *in situ* monitoring of plant VOC emission in real-time fashion.

RESULTS

Selection of sensing materials and performance of thiourea@rGO sensors

A large number of conductive and durable nanomaterials have been employed as flexible sensing materials.⁵⁶ Carbon-based materials possess low density, exceptional optical transparency, and superior chemical or electrochemical stability, and therefore are frequently selected as the sensing elements.^{18,57–59} Among various

carbon-based materials, graphene has a larger surface-area-to-volume ratio and improved conductivity than other carbon nanomaterials such as carbon dots and carbon nanotubes. We tested four potential carbon substrates in response to 10 ppm (*E*-2-hexenal, a C6 GLV known as a VOC biomarker for late blight.¹⁸ All carbon nanomaterials were functionalized with 1,3-dis[3,5-bis(trifluoromethyl)phenyl]thiourea (or thiourea for short), a chemical selector reported to form strong hydrogen bonds with electronegative elements such as carbonyl oxygen (Figure 1B).⁵⁴ Sensor elements were placed in a three-dimensional (3D)-printed gas chamber (4 × 3 × 1.2 cm) for sensing performance characterization using a three-way gas-mixing setup (Figure S2). We demonstrated that rGO showed the optimal and most reproducible sensor responses compared with graphene oxide (GO) and single-walled or multi-walled carbon nanotubes (SWCNTs or MWCNTs, respectively; Figure S3). Trends in the sensor response are consistent with the chemical and physical properties of different carbon materials: compared with GO and MWCNTs, rGO and SWCNTs have higher conductivity, larger surface areas, and less discrepancy in surface chemistry (higher product purity). As a comparison, pristine rGO without any surface functionalization showed nearly no response to the gas analyte (Figure S4). This result confirms that the specificity of the rGO sensors truly comes from the functional chemical ligands and therefore reduces the possible interference from the rGO itself. The mass ratio between thiourea ligand and rGO ($m_{\text{thiourea}}:m_{\text{rGO}}$) also affects the sensing performance. We found that 16.7 wt % of thiourea in the thiourea@rGO hybrids produced the largest signal response (Figure S5), which was used for all subsequent studies.

We then examined the sensing performance of the thiourea@rGO sensor toward four model plant VOCs, namely (*E*-2-hexenal, 1-hexenal, methyl jasmonate, and 2-phenylethanol, which have been reported as potential VOC diagnostic markers of *P. infestans*-infected tomato plants.¹⁸ The four model VOCs differ in multiple physical and chemical properties such as polarity, hydrophilicity, and nucleophilicity of particular atoms or functional groups, which reflects the complicated nature of emitted plant VOC mixtures under different stresses. The thiourea@rGO sensor displayed a quick response within the first 20 s of exposure (i.e., >90% of equilibrated response), and the positive electrical responses were totally reversible after purging with N₂ (Figure 2A). The electric resistance of thiourea@rGO sensor presented a nearly linear dependence on VOC concentrations (Figure S6A), with a limit of detection (LOD) ranging from ~0.13 ppm to 1.4 ppm (Figure S6B). Compared with our previously reported colorimetric sensor array,³⁴ the LODs of the wearable VOC sensors were improved by 2- to 10-fold for all tested VOCs except for (*E*-2-hexenal (Figure S6B).

Preparation and performance of AuNP@rGO sensors

To enhance the chemical diversity of the sensor array, we also integrated AuNP@rGO sensors based on halogen or hydrogen interactions with plant VOCs (Figure 1B). Six probe molecules (Figure S1B), including four halothiophenols (ITP [iodothiophenol], BPT [bromothiophenol], CTP [chlorothiophenol], and FTP [fluorothiophenol]), a nitrothiophenol (NTP; hydrogen interaction), and a methoxythiophenol (MTP; control) were first attached to the surface of AuNPs (Figure 1B), and then mixed thoroughly with rGO substrates using the ball-milling technique. It has been reported that halogen-bonding interactions can be formed between electropositive aryl halide-based selectors and electron donors such as pyridine or pyrrole, which induces negative changes in resistance as opposed to positive changes obtained by the thiourea@rGO sensor.²⁶ Since most plant VOCs are abundant in nitrogen- or oxygen-containing functional groups, those hydrogen or halogen-bonding

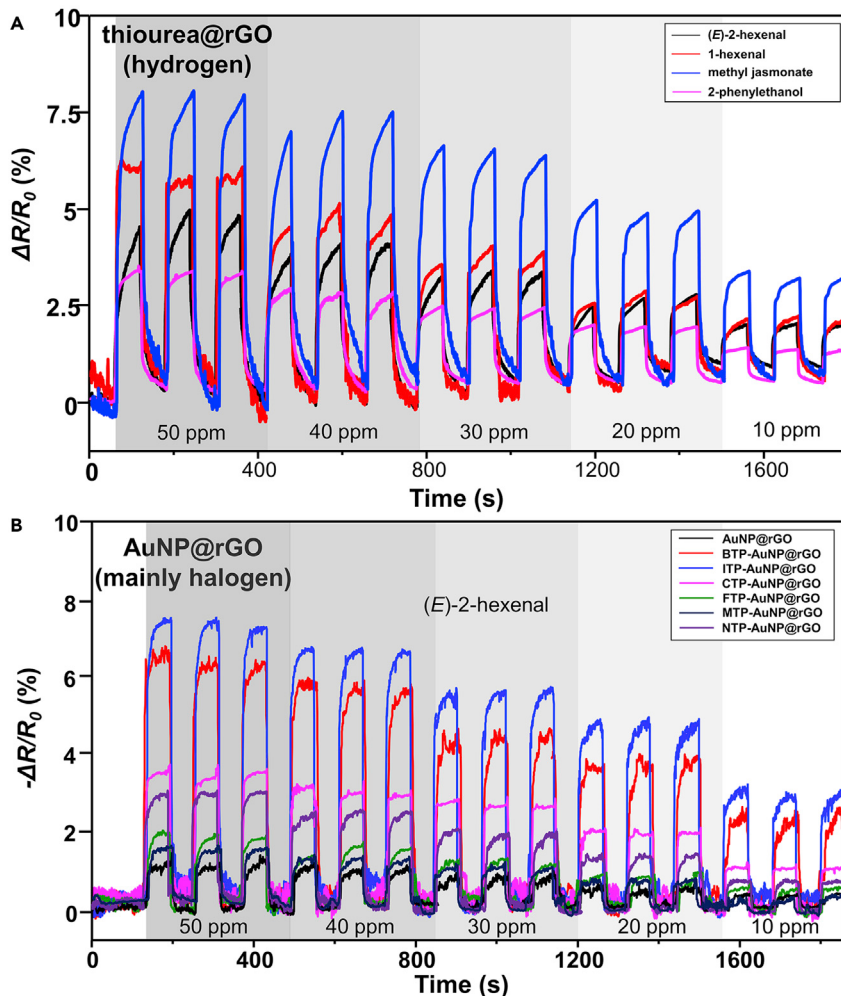


Figure 2. Reversibility of the chemiresistive rGO sensors

(A) Resistive responses of the thiourea@rGO sensors to four VOCs at 10–50 ppm range. Sensors were exposed to each concentration for 1 min followed by N_2 purging over three cycles.

(B) Resistive responses of uncapped or different capped AuNP@rGO sensors to (E)-2-hexenal at 10–50 ppm concentration range. Sensors were exposed to each concentration for 1 min followed by N_2 purging over three cycles.

mechanisms could possibly be applied for the recognition of multiple structurally similar plant VOCs. The mixing ratio of AuNP@ligand with the rGO substrate again has been optimized, which was determined to be 9.1 wt % of capped AuNPs for the AuNP@rGO sensors (Figures S7A and S7B). Transmission electron microscopy images of AuNP@rGO sensors with 1.8 wt % and 9.1 wt % of AuNPs are shown in Figures S7C and S7D, respectively, confirming the formation of AuNP@rGO nanohybrids. Taking advantage of the ultra-large surface area of AuNP-decorated rGO nanosheets, sensitive but reversible electrical responses were achieved by the AuNP@rGO sensors upon exposure to (E)-2-hexenal at the concentration range of 10–50 ppm (Figure 2B). The chemical diversity of different surface ligands anchored on the AuNP@rGO sensors offers the ideal cross-reactivity for the identification and discrimination of different plant volatiles. Similar to the aforementioned thiourea@rGO sensor, the signals of all AuNP@rGO sensors changed linearly as a function of VOC concentration (Figure S7A), and the four most responsive sensor elements

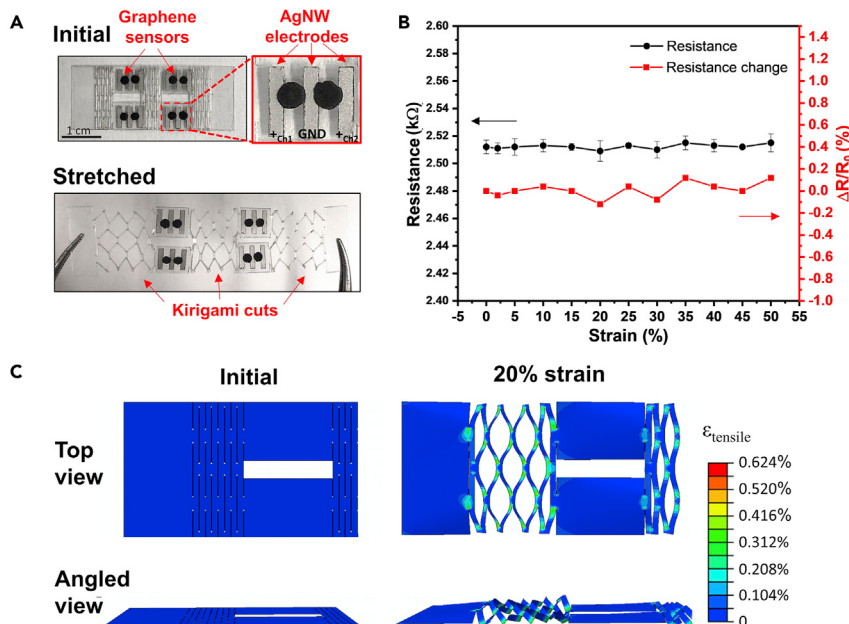


Figure 3. The sensor array patch and its mechanical stretchability

(A) Photographs of initial and stretched states of the wearable patch with contracted and extended kirigami structure.

(B) Resistance and relative resistance changes ($\Delta R/R_0$) of the sensor array patch with different degrees of applied strain. The error bars represent the standard deviation.

(C) Top and angled views showing FEA simulations of the principal stress distribution on the patch. Twenty percent strain was applied to simulate the deformation of the kirigami structure and “islands” for sensors. Note that due to symmetry, only the left half of the patch was simulated.

(i.e., iodo-, bromo-, chloro-, and nitro-substituted thiophenols) showed the LODs in the range of 0.17–3.9 ppm (Figure S8B). The sensing performance was quite comparable when using air or N₂ as the purging gas, indicating applicability of the sensor under normal ambient conditions (Figure S9).

Fabrication of an integrated wearable VOC sensor array patch

Next, we integrated rGO-based VOC sensors with soft silver nanowire (AgNW) electrodes, and developed a wearable sensor array patch that can be readily mounted on the plant leaf for real-time monitoring of plant VOCs (Figures 1 and 3). Due to their working principle, chemiresistive sensors are generally sensitive to mechanical strain. For on-plant applications, it is essential to minimize the sensor noise due to the mechanical strain induced by leaf vibration or growth. Given that the amplitude of the VOC signals ($\Delta R/R_0$) are within the range of 2%–8% (Figure 2), our design goal is to maintain nonspecific sensor signals due to mechanical perturbations below 0.2% in order to achieve a high signal-to-noise ratio. Toward this end, a stretchable sensor substrate, a kirigami-based structure, was adopted, which can effectively shield the sensors from the mechanical strain. Among a variety of structural candidates for stretchable substrates, kirigami design is widely employed in wearable devices. When stretched, out-of-plane deformation (e.g., lateral buckling) occurs on the kirigami plane, which effectively releases the applied in-plane strain.^{60–64}

Figure 3A shows the wearable sensor array patch that contains eight rGO sensors on four rigid regions (“islands”) connected with the stretchable kirigami structures

("bridges"), in the so-called island-bridge configuration (for details of sensor patch fabrication, see [experimental procedures](#)). In this configuration, the active sensing elements (functionalized rGO) were located on several separated and solid "islands," which protected the sensing materials from being deformed by the local mechanical strain. In contrast, the "bridge" structure is fully stretchable and bendable in multiple directions, particularly along or vertical to the main leaf vein. The sensor patch was made of a polyimide (PI) film. The kirigami structure was fabricated by CO₂ laser scribing. The kirigami cuts were designed to accommodate the uniaxial strain in the main leaf vein direction, where the strain may be introduced by bending or growth of leaves. During stretching in the longitudinal direction (main leaf vein direction), the kirigami structure would absorb most of the strain while the islands would take nearly zero strain. On the other hand, to release strain in the transverse direction during the longitudinal stretching (so-called Poisson's effect), several kirigami gaps were introduced between the sensor "islands" to reduce the bending effect. When stretching the sensor patch in the main leaf vein direction, the gaps will shrink and prevent the active sensor areas from compressing or decoupling from the leaf surface. [Figure 3B](#) shows the average resistance and the resistance change ($\Delta R/R_0$) of the eight fabricated sensors as functions of the applied strain, which indicates the stability of the resistance signal (i.e., $\pm 0.2\%$ fluctuation) in the range of 0%–50% strain. Finite element analysis (FEA) was also carried out to elucidate the strain effect. Due to the symmetry, only the left half of the patch was simulated. As shown in [Figure 3C](#), with the longitudinal strain of 20%, the maximum local strain in the island region is 0.104%, while in the kirigami structure it is 0.624%. This also showed that the out-of-plane deformation (angled view) plays a key role in the reduction of local strains in the kirigami structure ([Figure 3C](#)).

Apart from the mechanical perturbation, other environmental perturbations such as the variations in temperature or humidity were also investigated ([Figure S10](#)). The relationship of baseline rGO sensor signals (R_0) as a function of temperature and humidity is shown in [Figures S10A](#) and [S10B](#). With the increase of temperature, the resistance of ITP-AuNP@rGO decreases linearly ([Figure S10A](#)). The temperature coefficient of resistance (TCR) is estimated to be $-6.16 \times 10^{-3}/^\circ\text{C}$. TCR is calculated by $\text{TCR} = \frac{1}{R(T_0)} \frac{R(T) - R(T_0)}{T - T_0}$, where $R(T_0)$ is the resistance at T_0 (room temperature) and $R(T)$ is the resistance at T . On the other hand, the resistance of the same sensor increases monotonously with the increase of relative humidity ([Figure S10B](#)). To further evaluate the VOC-sensing performance under different temperature (10°C, 25°C, and 40°C) and humidity (30%, 50%, and 80%) conditions, we tested the ITP-AuNP@rGO sensor under exposure to 50 ppm hexenal. The cyclic responses of the VOC sensor (alternate hexenal and N₂) were recorded ([Figures S10C–S10F](#)). As shown in [Figure S10C](#), the baseline resistance values (R_0) of the sensor decreases as the temperature increases, consistent with the results in [Figure S10A](#). The resistance change ($\Delta R/R_0$) increases slightly with increased temperature ([Figure S10D](#)), probably due to the improved electron transfer at a higher temperature. In the humidity experiment, the baseline resistance values (R_0) of the sensor increase as a function of external humidity ([Figure S10E](#)), which is consistent with the result in [Figure S10B](#). The resistance change ($\Delta R/R_0$) of the sensor decreases slightly with the increase in humidity ([Figure S10F](#)). This may be due to the increased competitive binding between water and VOC molecules in a higher-humidity environment. These studies suggested that although temperature and humidity do slightly interfere with VOC detection, use of resistance change ($\Delta R/R_0$) instead of absolute resistance (R_0) and a precalibrated temperature and humidity function would greatly minimize such interference.

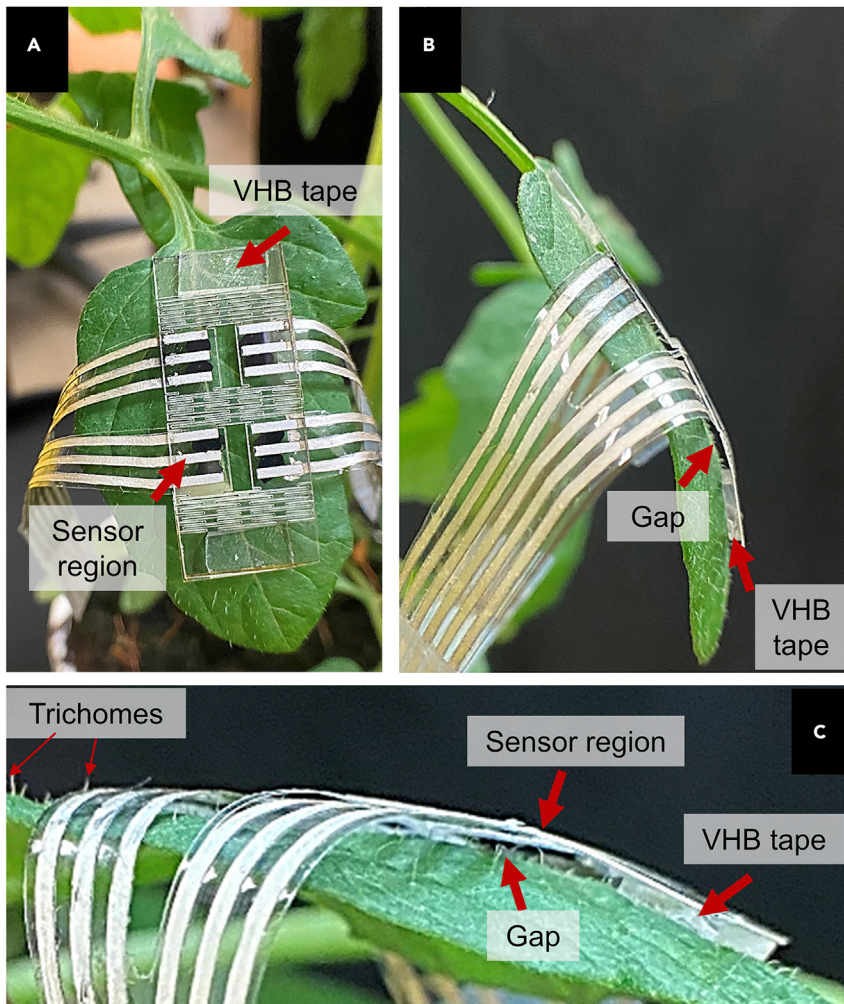


Figure 4. Photographs of sensor attachment on the tomato leaf

- (A) Top view of the wearable sensor patch on the leaf.
(B) Side view of the sensor on the leaf.
(C) Zoom-in view of the interface between the sensor patch and the leaf.

The electrodes of the wearable sensor were made of AgNW percolation network because of its high electrical conductivity and mechanical flexibility/stretchability.^{65–68} Flexible interconnect ribbon cables were used to connect the sensor array and the external electronics (Figure S11). A convenient feature is that the ribbon cables were also made of AgNWs, following the same fabrication method as the AgNW electrodes in the sensor array. The cables were attached to the AgNW electrodes using anisotropic conductive film tape (Figure S11A). Figure S11B shows a sensor patch with eight sensors and two interconnects, and Figure S11C shows the sensor patch mounted on a living tomato plant. The imperceptible sensor patch was attached to the upper surface of a leaf with the sensing materials facing the leaf (with a spacing of ~0.6 mm), which corresponds to a gas chamber volume of ~ $<2\text{ cm}^3$ between the wearable sensor and the leaf. As shown in Figure 4, a double-sided tape (3M VHB) was used to mount the wearable sensor on the surface of the tomato leaves. The tape is ~0.6 mm thick, which keeps a gap between the sensor substrate and the leaf. Even when the leaf bends (as shown in Figure 4B), the gap is still large

enough to isolate the active sensor materials from the leaf surface. Moreover, the tiny hairs on the surface of the tomato leaves, which are trichomes of the tomato leaves (Figure 4C), can also help keep a small distance and prevent direct contact between the sensor and the leaf.

Figure S12 shows the strain insensitivity of the sensors (up to 20% strain) in both air and N₂. The resistances of two types of sensors (ITP-AuNP@rGO and BTP-AuNP@rGO) slightly fluctuated in air while remaining almost unchanged in pure N₂ (Figure S12). The air was supplied by a compressed dry air system, and the N₂ was supplied by an N₂ gas tank. The sensor signals showed slightly more fluctuation in the air, probably due to the trace amount of VOC contaminants in the air. Figure S13 illustrates the stability of the ITP-AuNP@rGO sensor over 1,600 loading-unloading cycles in air and N₂. No noticeable resistance change was detected throughout the test (Figure S13). These results clearly demonstrated the robustness and stability of the wearable sensor array under mechanical loadings. Apart from the mechanical stability, the lifetime of the sensor was also characterized by measuring the cyclic response curves of the functionalized sensor on the first day of preparation and after 90 days of shelf time (Figure S14). No obvious differences in sensor baseline or sensor response pattern were observed before and after 90 days of storage in air, which indicates the excellent stability of the sensor array (Figure S14).

Discrimination of individual plant VOCs

We then tested the wearable sensor array for the discrimination of a wide range of common plant volatiles, including two characteristic late blight markers ((E)-2-hexenal and 2-phenylethanol), four GLVs ((Z)-3-hexenal, 1-hexenal, (E)-2-hexenol, and (E)-2-hexenyl acetate), two phytohormones (methyl jasmonate and methyl salicylate), and five aromatics (benzaldehyde, 4-ethylguaiacol, 4-ethylphenol, indole, and benzothiazole). All 13 VOCs were generated by the gas-mixing system at a concentration of 10 ppm (Figure S2). Figures 5A and 5B are the original sensor response and heatmap representation of the sensor response, respectively. The results demonstrated that an eight-channel VOC sensor array could produce a unique response pattern upon exposure to each analyte within 1 min of exposure. A multivariate statistical approach, principal component analysis (PCA), was performed to extract the dimensionality of the data library. Using the first three principal components accounting for >95% of the total variance, we were able to distinguish all 13 plant VOCs at 10 ppm concentration from the control (N₂) in 42 out of 43 trials in total (Figure 5C). The overall classification accuracy is 97.6% (42/43). The discrimination capability of the sensor patch is dependent on the number of active VOC sensor elements included in the array. If with four sensor elements, the same group of plant VOCs cannot all be classified by the sensor array (Figure S15).

Real-time profiling of VOCs on living tomato plants

The sensor patch was finally attached to live tomato plants to test its sensing performance. The anti-disturbance properties of the sensor patch were evaluated by introducing different external perturbations to the subject plant, such as wind blowing and mechanical touching or shaking (Figure 6). As shown in Figure 6A, the resistance of the sensor fluctuated <0.5% in amplitude when a fan blew the subject plant with a wind speed of ~1.5 m s⁻¹ from 1 m away. The resistance change was likely due to the shaking of the electric circuit (e.g., the ribbon cable). The resistance returned to the initial value after the fan was turned off. The influence of mechanical vibration of the subject leaf and stem on the sensor signals was also investigated. Figure 6B shows that gentle touching of the leaf would not change the resistance of the sensor patch (gray zone), while shaking the stem introduced a very small oscillation to the

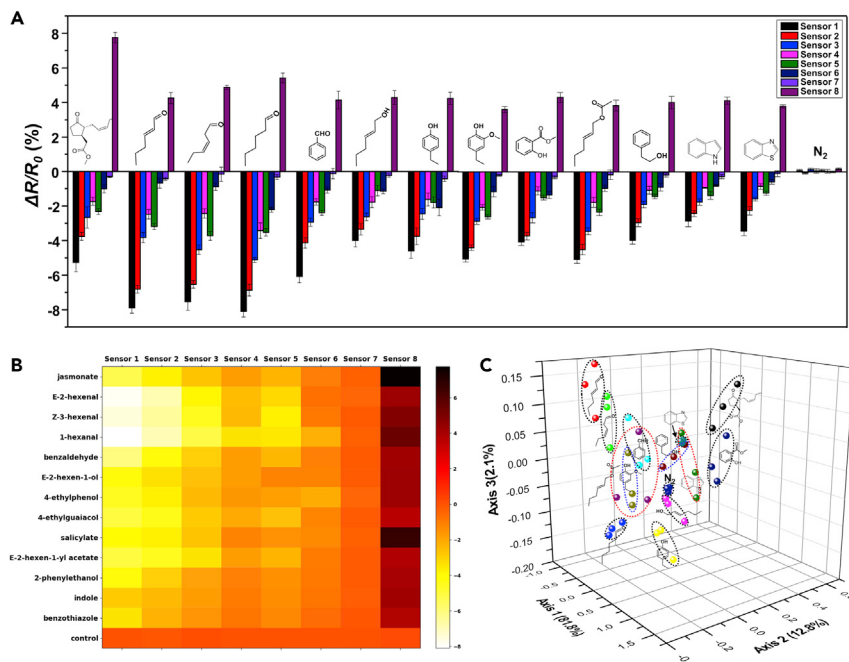


Figure 5. Multiplexed detection and analysis of plant VOCs

(A) Responses of eight chemiresistive sensors upon exposure to 13 plant VOCs at 10 ppm plus the N₂ control. The eight sensors are ITP-AuNP@rGO (#1), BTP-AuNP@rGO (#2), CTP-AuNP@rGO (#3), FTP-AuNP@rGO (#4), NTP-AuNP@rGO (#5), MTP-AuNP@rGO (#6), AuNP@rGO (#7), and thiourea@rGO (#8). The abbreviations for different ligands are as follows: ITP, 4-iodothiophenol; BTP, 4-bromothiophenol; CTP, 4-chlorothiophenol; FTP, 4-fluorothiophenol; NTP, 4-nitrothiophenol; MTP, 4-methoxythiophenol. The error bars represent the standard deviation.

(B) Heatmap of the eight-channel sensor response toward 13 plant VOCs and N₂ control.
(C) The corresponding PCA plot.

resistance signal (green zone). These results suggested that the wearable sensor system is reliable and robust under a variety of external disturbing loads.

The wearable sensor patch was then tested to monitor abiotic stresses of tomato plants induced by mechanical cutting at different locations (Figure 7). Figure 7A illustrates the cutting locations: either at the stem (red dashed box in Figures 7A and 7B) or at the leaf underneath the sensor (yellow dashed box in Figures 7A and 7C). Figures 7B and 7C are the magnified pictures showing the cuts from the backside of the leaf with a sensor patch on the top side. For the stem cut, Figure 7D shows that the resistances increased slowly within the first 12 h after cutting and then reached a plateau. In the case of the leaf cut that was directly underneath the sensor patch, there was an instant increase in resistance in response to the cut (within the first 1 h), and the sensor signals gradually became steady after a few hours. This may be due to the immediate emission of a large amount of VOCs induced by the mechanical damage to the leaf. In contrast, the stem cut seemed to induce a much slower VOC-emission rate, and also the location of the stem cut is far away from the sensor patch, both of which might contribute to the minor response of sensor signals.

Finally, a wearable sensor array was applied to monitor the biotic stresses of tomato plants induced by the infection of *P. infestans* in real time (Figure 8). The sensor array consisting of multiple AuNP@rGO sensors was attached to healthy tomato plants that were grown in a growth chamber to provide a controlled temperature and

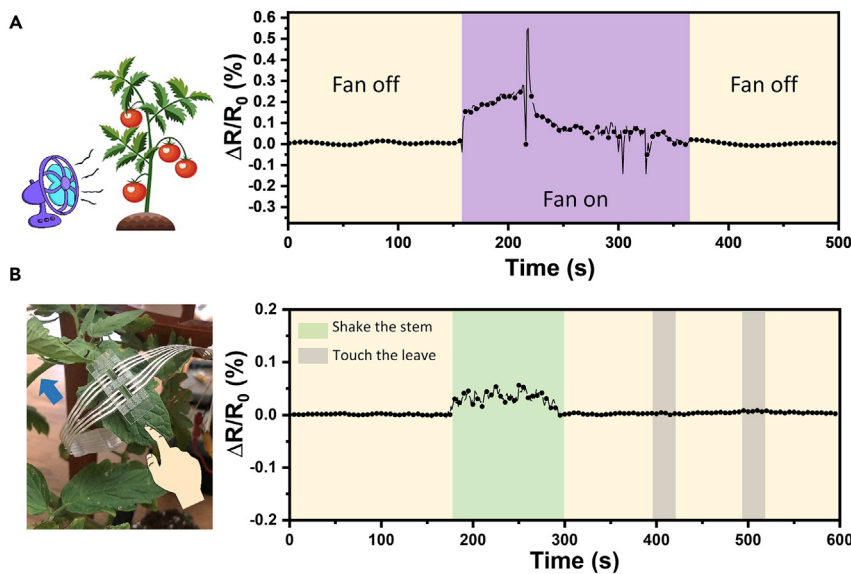


Figure 6. Anti-perturbation properties of the wearable sensor on living tomato plants

Sensor resistance response curves due to (A) wind disturbance at $\sim 1.5 \text{ m s}^{-1}$ speed and (B) touch disturbance on the leaf or stem.

humidity environment for the experiments (Figure 8A). After 15 h of recording, when the VOC response was in its steady state, inoculation of *P. infestans* was performed by spraying the whole plant with *P. infestans* sporangia suspensions ($\sim 5,000 \text{ sporangia mL}^{-1}$). As shown in Figure 8B, the sensor response was stable for the first 15 h. After the inoculation of *P. infestans*, small fluctuations of the sensor signals were observed in the first ~ 35 h. A more significant signal increase was observed starting at ~ 90 h (within 4 days) after inoculation, which is attributed to the release of characteristic VOC molecules due to the propagation of *P. infestans* infection. It is worth mentioning that two watering events at 10 h and 50 h after inoculation did not introduce significant signal interference to the sensors. At ~ 115 h after inoculation, some circular gray spots and water-soaked lesions were visible on the leaves. At this time, the sensor signals gradually reached a plateau, indicating that the VOC-emission profile of the tomato leaf was completely changed by the infection of *P. infestans*, and a new equilibrium was reached (Figure 8B). These results confirm the ability of the developed sensor array to capture plant disease infection at the early stage (e.g., within 4 days post inoculation) by continuous multiplexed VOC profiling.

DISCUSSION

In recent decades, array-based sensors such as electronic noses have shown a wide range of applications especially in environmental, agricultural, and food analysis.^{69–71} Pattern recognition is widely used in the analysis of the multidimensional data matrices for identification and discrimination of single targets or analyte mixtures. Compared with other gas-detection methods such as conventional GC-MS, array-based gas sensors are inexpensive, portable, easy to deploy, and therefore well suited for field applications.

However, only few sensor technologies (including e-noses) intended for agricultural applications are capable of performing real-time monitoring of physiological states of plants,^{44,72} with the majority not satisfying the demand for continuous and long-term testing in the field. The recently developed plant-wearable sensors, on the

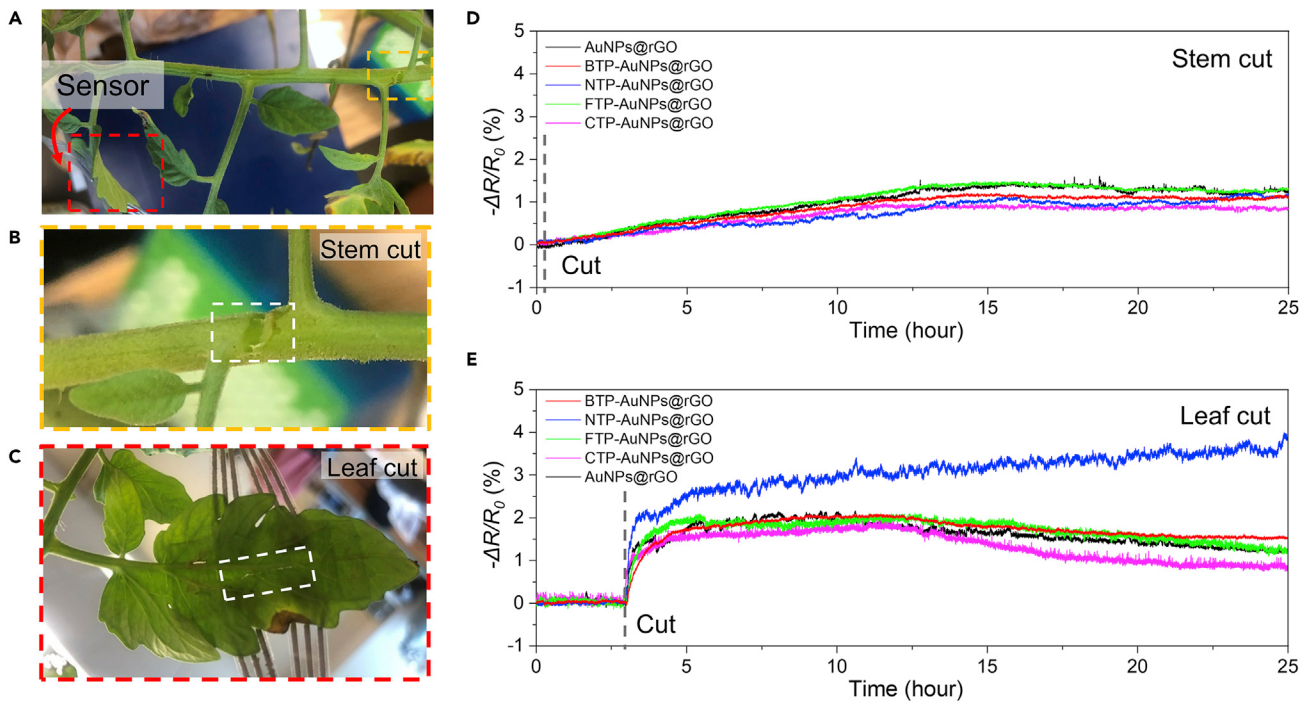


Figure 7. Real-time monitoring of abiotic plant stresses due to mechanical damage

- (A) Photograph of the location of the wearable sensor (yellow dashed box) and two mechanical-damage sites.
- (B and C) Zoomed-in photographs of the mechanical cut on the stem (B) and leaf (C), respectively.
- (D) Real-time response curves of a 5-channel sensor array after mechanical cut on the stem.
- (E) Response curves of the 5-channel sensor array after mechanical cut on the leaf.

other hand, are limited by their sensing capability only to environmental or mechanical parameters, such as humidity, temperature, light, and growth rate.^{42,47,48} In contrast, the demonstrated wearable plant sensor in this work is able to track more biologically relevant markers such as plant VOCs for the first time to better decode plant stresses. This new wearable VOC sensor patch employs chemically specific and nanoscale sensing elements consisting of cross-reactive rGO-based gas sensors, which greatly enhanced the detection sensitivity, multiplexity, and chemical specificity. We systematically characterized the response of the individual rGO sensors (Figure 2), the performance of the sensor array as a whole (Figure 5), their mechanical stability (Figures S12 and S13), and anti-interference properties when mounted on living plants (Figure 6). While temperature and humidity may potentially influence the VOC signals, the interference can be minimized by using the ratiometric signal ($\Delta R/R_0$) instead of absolute resistance response (R_0) and implementing a precalibrated function for temperature and humidity (Figure S10). We further demonstrated that the wearable sensor array is accurate, specific, and reproducible in predicting relative VOC emissions generated from several types of biotic or abiotic stresses, including *P. infestans* infection and mechanical cutting (Figures 7 and 8), which proves its utility as a new alternative to other available sensor techniques for in-field and on-plant identification of unhealthy plants.

The main innovation of this work lies in two aspects. First, we bring VOC-sensing capability to a plant-wearable sensor, for the first time, by using a wide range of chemiresistive-based sensing materials modified with different functional chemical ligands to achieve desired chemical sensitivity and specificity. The chemical ligands

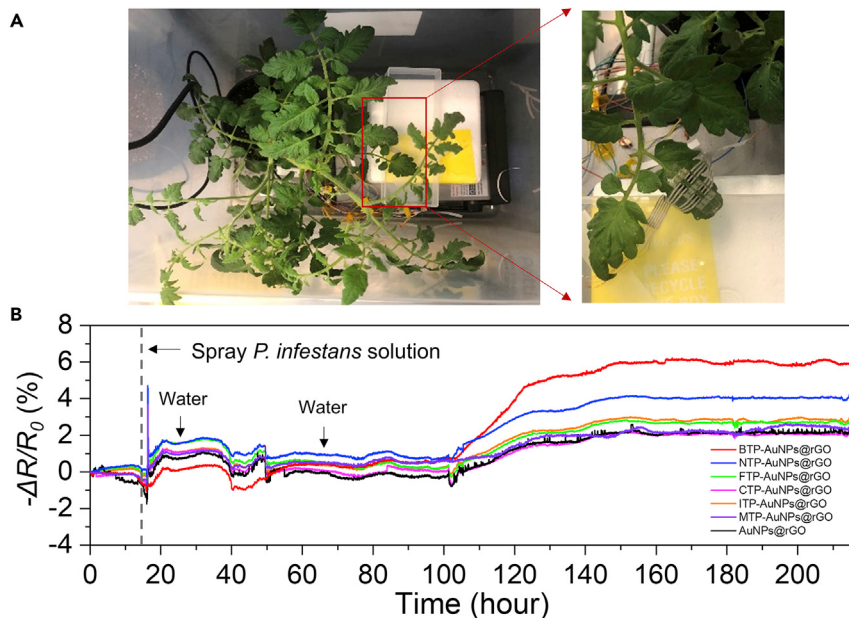


Figure 8. Real-time monitoring of biotic plant stresses due to pathogen infection

(A) Photographs of wearable sensor array patch attached to the tomato leaf.
(B) Real-time response curves of the sensor array in response to the inoculation of *P. infestans*.

on the surface of rGO sensor substrates consist of a thiourea compound and different *para*-substituted, thiophenol-capped AuNPs (bearing -I, -Br, -Cl, and -F groups) as selective chemical receptors that can detect leafy ketones and aldehydes, respectively. The two groups of ligands also represent two different reversible interactions with leaf VOCs, namely hydrogen interaction and halogen interaction. We³⁴ and other groups^{17,19} have previously found that the emission level of aldehydes (e.g., 1-hexanal, (E)-2-hexanal, and (Z)-3-hexanal) was frequently elevated for stressed tomato plants (either pathogen infection or mechanical damage). As such, the wearable VOC sensor array is rationally designed to have desired chemical ligands to detect those stress VOC makers. Two additional chemical ligands (NTP and MTP) were also included in the sensor array as internal controls to halothiophenols.

Second, we have designed a unique stretchable substrate comprising a kirigami structure and soft AgNW electrodes to mitigate strain interface to the VOC sensors. Several strategies such as kirigami cuts, “island-bridge” design, and flexible interconnect ribbon cables were adapted to ensure its signal insensitivity and stability against external perturbations that could occur during field deployment, e.g., wind blowing, mechanical touching, or the strain induced by the leaf growth itself.

Although graphene-based sensors have been extensively studied in human health monitoring,^{73,74} their potential applications in agriculture have rarely been explored. The active sensing ligands (e.g., thiourea or functionalized AuNPs) used in this research are immobilized on the highly conductive rGO surface layer and packaged in a stretchable polymeric matrix, whose electrical signals can be easily recorded and quantified by a low-cost digital multimeter, or a multichannel front-end electronic circuit with wireless communication that is currently under development. The detection specificity of chemiresistive gas sensors was achieved by diversifying

functional groups anchored on the surface of rGO or AuNPs. The concept of nanoparticle-enhanced gas sensing that can provide ultra-sensitivity and chemical specificity has been well established in our latest studies.³⁴ In this work, the AuNPs enable the introduction of ultra-large surface area and versatile surface functionalities to probe extensively their hydrogen- or halogen-bonding interactions with a broad range of gaseous targets that are particularly rich in oxygen- or nitrogen-containing functional groups.

Conclusion

In conclusion, we have developed a field-deployable wearable sensor platform that can be attached to plant leaves for noninvasive, continuous monitoring of VOCs arising from common plant stresses, including pathogen infection and abiotic stresses. The multiplexed chemical sensor array is built upon functionalized chemiresistive nanomaterials to target various plant volatile markers with the detection limit down to low-ppm or sub-ppm levels. With only eight sensing elements, the sensor array has already demonstrated its remarkable performance in simultaneous detection and classification of 13 individual plant volatiles. By integrating the rGO sensors with soft AgNW electrodes using the stretchable island-bridge configuration and kirigami structures, real-time monitoring and forecast of tomato late blight were achieved as early as 4 days post inoculation. Moreover, the integrated sensor platform can indicate abiotic stresses such as physical damage in a much faster fashion (within 1 h) by detecting continuously the VOC emissions from the damaged plant tissue. The rGO sensors do respond to humidity and temperature slightly, which requires a careful calibration step to minimize the environmental interference. Nevertheless, given the unprecedented chemical sensitivity, specificity, portability (~0.7 g per sensor patch), and cost-effectiveness (estimated cost \$1.1 per patch), this integrated chemiresistive gas sensor platform could be a powerful alternative to other diagnostic tools available for long-term monitoring of plant health in the field.

EXPERIMENTAL PROCEDURES

Resource availability

Lead contact

Further information and requests for resources and reagents should be directed to and will be fulfilled by the lead contact, Qingshan Wei (qwei3@ncsu.edu).

Materials availability

All unique/stable reagents generated in this study are available from the lead contact with a completed Materials Transfer Agreement.

Data and code availability

The datasets supporting the current study have not been deposited in a public repository but are available from the corresponding author on request.

Materials and reagents

All reagents and materials were analytical-reagent grade and used without further purification. GO, rGO, SWCNTs, MWCNTs, and tested plant VOCs generated from solvents including (*E*)-2-hexenal, 2-phenylethanol, (*Z*)-3-hexenal, 1-hexenal, (*E*)-2-hexenol, (*E*)-2-hexenyl acetate, methyl jasmonate, methyl salicylate, benzaldehyde, 4-ethylguaiacol, 4-ethylphenol, and benzothiazole were purchased from Sigma-Aldrich (St. Louis, MO, USA). Polyimide resin was purchased from Fujifilm (Valhalla, NY, USA). Ag nanowires were synthesized by a modified polyol method,⁷⁵ and the produced Ag nanowires were suspended in ethanol for further use.

Preparation of the rGO-Based sensors

Two types of rGO-based sensors were prepared, namely thiourea@rGO sensors and AuNP@rGO sensors. In brief, AuNP was synthesized by a traditional sodium citrate reduction method.⁷⁶ Two hundred microliters of 1 μ M ligand solutions were added to AuNPs, making a total solution volume of 2 mL. The reaction between AuNPs and chemical ligands was continued for 8 h at room temperature with mild stirring before centrifugation and collection of the final product. Before measuring the UV-visible spectrum, ligand-capped AuNP was dispersed in Milli-Q water. For preparation of AuNP@rGO sensors, rGO was mixed with functionalized AuNPs at different mass ratios. For thiourea@rGO-based sensors, thiourea was directly added to rGO at different mass ratios.

Fabrication of the wearable sensor patch

The fabrication of a chemiresistive sensor patch started with patterning Ag nanowire electrodes on glass slides. A hard mask was adhered onto the glass slide and patterned by a laser cutter (VLS6.60; Universal Laser Systems). Next, the Ag nanowire solution was drop-cast onto the mask and dried under vacuum. Polyimide resin was subsequently spin-coated on the Ag nanowire electrodes and cured under ambient conditions. Laser cutting was used again for patterning the kirigami structure of the patch. The fabricated thin-film platform was then inverted and the electrodes exposed upward. Finally, ~20 mg of the as-prepared AuNP@rGO or thiourea@rGO sensing materials were drop-cast between the paired electrodes and dried thoroughly under vacuum prior to gas measurement. The size of the entire sensor patch is 12 mm \times 30 mm. Each of the four sensor islands is 5.7 mm \times 5.2 mm in size. The gap that separates each two sensor islands is 1.6 mm wide in the transverse direction. The size of each Ag nanowire electrode is 0.8 mm \times 4 mm, and the spacing between each pair of electrodes for loading sensor elements is 0.5 mm.

Gas-sensing studies

The chemiresistive sensor array was placed in a 3D-printed gas chamber (5 \times 4 \times 2.5 cm) for laboratory gas-sensing experiments (Figures S2A–S2C); resistance change of the tested electrode loaded with certain sensing material was monitored by a digital multimeter (Agilent 34465; Keysight) and recorded by the software BenchVue 2018. VOC vapor was generated by bubbling N₂ through the VOC liquid. Using both air and N₂ as purging gas resulted in similar and repeatable sensor responses (Figure S16). Gas mixtures were prepared according to previous methods as shown in Figure S2D. In brief, mass flow controllers (MKS) were used to obtain gas streams with the desired concentration (10–50 ppm), total flow rate (500 sccm), and humidity (50% relative humidity) by mixing the proper portion of saturated vapor of the liquid analyte with dry (0% relative humidity) and wet (100% relative humidity) nitrogen gas. The sensor arrays were exposed to VOC vapor at fixed concentration for 1 min, followed by pure N₂ purging for another 1 min for baseline recovery; alternate exposure to the analyte and the control was repeated for three cycles.

Data processing and principal component analysis

The resistance response was normalized as $\Delta R/R_0$. ΔR and R_0 are the resistance change under the exposure to VOCs and the baseline resistance under N₂ stream, respectively. PCA was calculated from the data matrix, in which the columns were the amplitudes from each sensing element and the rows represented different VOC targets. Measurements of each VOC were repeated in triplicate.

Living plant monitoring and inoculation of plant leaves

Real-time recording of resistive changes of multiple electrodes on the sensor array patch fixed on plant leaves was monitored by a multichannel digital multimeter (DAQ970A; Keysight). Infected tomato plants were collected from Dr. Jean Ristaino's lab in the Department of Entomology and Plant Pathology, North Carolina State University. These plants were inoculated using a US-23 genotype of *P. infestans* (isolate NC 14-1). Tomato seedlings were purchased from a local supermarket and cultivated at room temperature ($25^{\circ}\text{C} \pm 2^{\circ}\text{C}$) under ~ 13 h of light per day. One milliliter of deionized water was sprayed on the abaxial side of the vertically placed leaves to collect *P. infestans* sporangia. The runoff liquid from the leaves contains sporangia of *P. infestans*, which was collected in a beaker. A hemocytometer (Hausser Scientific) was used to measure the number of sporangia per milliliter of collected solution.¹⁴ Living plants were inoculated by spraying 2 mL of *P. infestans* sporangia suspensions ($\sim 5,000$ sporangia mL^{-1}) onto the leaves.

SUPPLEMENTAL INFORMATION

Supplemental information can be found online at <https://doi.org/10.1016/j.matt.2021.06.009>.

ACKNOWLEDGMENTS

This work was supported by NCSU Chancellor's Faculty Excellence Program, the Kenan Institute for Engineering, Technology and Science (KIETS), NCSU Game-Changing Research Incentive Program for the Plant Science Initiative (GRIP4PSI), NCSU Center for Human Health and the Environment (CHHE) Pilot Project Award, USDA (no. 2019-67030-29311), USDA APHIS Farm Bill grant (no. 3.0096), and NSF (no. 1728370). Z.L. also acknowledges the financial support from the National Natural Science Foundation of China (no. 22076125), Natural Science Foundation of Guangdong Province (no. 2021B1515020106), and Guangdong Young Talents Project (no. 2019KQNCX218). We also thank Zeya Wang from Rice University for heatmap analysis.

AUTHOR CONTRIBUTIONS

Z.L., Y.L., Y.Z., and Q.W. designed the experiments. Z.L. and O.H. prepared and optimized the chemiresistive sensors. Y.L. and S.Y. designed and fabricated the wearable sensor patch. Z.L., Y.L., and O.H. carried out the VOC-sensing experiments and analyzed the data. J.B.R. provided the *P. infestans* strains, and R.P. prepared *P. infestans* inoculum for inoculation of tomato leaves. S.W. conducted the FEA simulation for the sensor patch. Z.L., Y.L., O.H., Y.Z., and Q.W. wrote the manuscript. All authors contributed to the editing of the manuscript.

DECLARATION OF INTERESTS

The authors have a pending patent application related to this work.

Received: February 25, 2021

Revised: May 13, 2021

Accepted: June 3, 2021

Published: July 7, 2021

REFERENCES

- Ristaino, J.B., Cooke, D.E.L., Acuña, I., and Muñoz, M. (2020). The threat of late blight to global food security. In *Emerging Plant Diseases and Global Food Security*, J.B. Ristaino and A. Records, eds. (American Phytopathological Society Press), pp. 101–132.
- Dremann, S.. A Plant Killer with Huge Economic Impact. <https://palaltonline.com/>
- Oerke, E.C. (2005). Crop losses to pests. *J. Agric. Sci.* 144, 31–43.

4. Hussain, S., Lees, A.K., Duncan, J.M., and Cooke, D.E.L. (2005). Development of a species-specific and sensitive detection assay for *Phytophthora infestans* and its application for monitoring of inoculum in tubers and soil. *Plant Pathol.* 54, 373–382.
5. Lees, A.K., Sullivan, L., Lynott, J.S., and Cullen, D.W. (2012). Development of a quantitative real-time PCR assay for *Phytophthora infestans* and its applicability to leaf, tuber and soil samples. *Plant Pathol.* 61, 867–876.
6. Trout, C.L., Ristaino, J.B., Madritch, M., and Wangsomboondee, T. (1997). Rapid detection of *Phytophthora infestans* in late blight-infected potato and tomato using PCR. *Plant Dis.* 81, 1042–1048.
7. Skottrup, P., Nicolaisen, M., and Justesen, A.F. (2007). Rapid determination of *Phytophthora infestans* sporangia using a surface plasmon resonance immunosensor. *J. Microbiol. Methods* 68, 507–515.
8. Harrison, J.G., Lowe, R., and Duncan, J.M. (1991). Use of ELISA for assessing major gene resistance of potato leaves to *Phytophthora infestans*. *Plant Pathol.* 40, 431–435.
9. ImmunoComb. <https://orders.agdia.com/pathogen-tests/immunostrip-tests>.
10. Ristaino, J.B., Saville, A.C., Paul, R., Cooper, D.C., and Wei, Q. (2020). Detection of *Phytophthora infestans* by loop-mediated isothermal amplification, real-time lamp, and droplet digital PCR. *Plant Dis.* 104, 708–716.
11. Khan, M., Li, B., Jiang, Y., Weng, Q., and Chen, Q. (2017). Evaluation of different PCR-based assays and lamp method for rapid detection of *Phytophthora infestans* by targeting the ypt1 gene. *Front. Microbiol.* 8, 1920.
12. Li, Z., Yu, T., Paul, R., Fan, J., Yang, Y., and Wei, Q. (2020). Agricultural nanodiagnostics for plant diseases: recent advances and challenges. *Nanoscale Adv.* 2, 3083–3094.
13. Paul, R., Ostermann, E., and Wei, Q. (2020). Advances in point-of-care nucleic acid extraction technologies for rapid diagnosis of human and plant diseases. *Biosens. Bioelectron.* 169, 11592.
14. Paul, R., Saville, A., Hansel, J., Ye, Y., Ball, C., Williams, A., Chang, X., Chen, G., Gu, Z., Ristaino, J., and Wei, Q. (2019). Extraction of plant DNA by microneedle patch for rapid detection of plant diseases. *ACS Nano* 13, 6540–6549.
15. Holopainen, J.K., and Gershenson, J. (2010). Multiple stress factors and the emission of plant VOCs. *Trends Plant Sci.* 15, 176–184.
16. Scala, A., Allmann, S., Mirabella, R., Haring, M.A., and Schuurink, R.C. (2013). Green leaf volatiles: a plant's multifunctional weapon against herbivores and pathogens. *Int. J. Mol. Sci.* 14, 17781–17811.
17. Butterly, R.G., Ling, L.C., and Light, D.M. (1987). Tomato leaf volatile aroma components. *J. Agr. Food Chem.* 35, 1039–1042.
18. Laithawornkitkul, J., Jansen, R.M.C., Smid, H.M., Bouwmeester, H.J., Muller, J., and van Bruggen, A.H.C. (2010). Volatile organic compounds as a diagnostic marker of late blight infected potato plants: a pilot study. *Crop Prot.* 29, 872.
19. Raghava, T., Ravikumar, P., Hegde, R., and Kush, A. (2010). Spatial and temporal volatile organic compound response of select tomato cultivars to herbivory and mechanical injury. *Plant Sci.* 179, 520–526.
20. Aksenen, A.A., Novillo, A.V.G., Sankaran, S., Fung, A.G., Pasamontes, A., Martinelli, F., Cheung, W.H.K., Ehsani, R., Dandekar, A.M., and Davis, C.E. (2013). Volatile organic compounds (VOCs) for noninvasive plant diagnostics. In *Pest Management with Natural Products*, 1141. ACS Symposium Series (American Chemical Society), pp. 73–95.
21. Jansen, R.M., Hofstee, J.W., Wildt, J., Verstappen, F.W., Bouwmeester, H.J., and van Henten, E.J. (2009). Induced plant volatiles allow sensitive monitoring of plant health status in greenhouses. *Plant Signal. Behav.* 4, 824–829.
22. Jansen, R.M., Wildt, J., Kappers, I.F., Bouwmeester, H.J., Hofstee, J.W., and van Henten, E.J. (2011). Detection of diseased plants by analysis of volatile organic compound emission. *Annu. Rev. Phytopathol.* 49, 157–174.
23. Sharma, R., Zhou, M., Hunter, M.D., and Fan, X. (2019). Rapid in situ analysis of plant emission for disease diagnosis using a portable gas chromatography device. *J. Agric. Food Chem.* 67, 7530–7537.
24. Mustafa, M.S., Husin, Z., Tan, W.K., Mavi, M.F., and Farook, R.S.M. (2019). Development of automated hybrid intelligent system for herbs plant classification and early herbs plant disease detection. *Neural Comput. Appl.* 32, 11419–11441.
25. Chalupowicz, D., Veltman, B., Drobys, S., and Eltzov, E. (2020). Evaluating the use of biosensors for monitoring of *Penicillium digitatum* infection in citrus fruit. *Sens. Actuators. B. Chem.* 311, 12896.
26. Weis, J.G., Ravnsbaek, J.B., Mirica, K.A., and Swager, T.M. (2015). Employing halogen bonding interactions in chemiresistive gas sensors. *ACS Sens.* 1, 115–119.
27. Wilson, A.D., and Baietto, M. (2009). Applications and advances in electronic-nose technologies. *Sensors* 9, 5099–5148.
28. Cui, S., Ling, P., Zhu, H., and Keener, H.M. (2018). Plant pest detection using an artificial nose system: a review. *Sensors* 18, 378.
29. Cellini, A., Blasioli, S., Biondi, E., Bertaccini, A., Braschi, I., and Spinelli, F. (2017). Potential applications and limitations of electronic nose devices for plant disease diagnosis. *Sensors* 17, 2596.
30. Askim, J.R., Mahmoudi, M., and Suslick, K.S. (2013). Optical sensor arrays for chemical sensing: the optoelectronic nose. *Chem. Soc. Rev.* 42, 8649–8682.
31. Escobedo, C. (2013). On-chip nanohole array based sensing: a review. *Lab. Chip.* 13, 2445–2463.
32. Li, Z., Askim, J.R., and Suslick, K.S. (2019). The optoelectronic nose: colorimetric and fluorometric sensor arrays. *Chem. Rev.* 119, 231–292.
33. You, C.C., Miranda, O.R., Gider, B., Ghosh, P.S., Kim, I.B., Erdogan, B., Krovi, S.A., Bunz, U.H., and Rotello, V.M. (2007). Detection and identification of proteins using nanoparticle-fluorescent polymer 'chemical nose' sensors. *Nat. Nanotechnol.* 2, 318–323.
34. Li, Z., Paul, R., Ba Tis, T., Saville, A.C., Hansel, J.C., Yu, T., Ristaino, J.B., and Wei, Q. (2019). Non-invasive plant disease diagnostics enabled by smartphone-based fingerprinting of leaf volatiles. *Nat. Plants* 5, 856–866.
35. Yao, S., Swetha, P., and Zhu, Y. (2018). Nanomaterial-enabled wearable sensors for healthcare. *Adv. Healthc. Mater.* 7, 1700889.
36. Yao, S., Ren, P., Song, R., Liu, Y., Huang, Q., Dong, J., O'Connor, B.T., and Zhu, Y. (2020). Nanomaterial-enabled flexible and stretchable sensing systems: processing, integration, and applications. *Adv. Mater.* 32, e1902343.
37. Lipomi, D.J., Vosgueritchian, M., Tee, B.C., Hellstrom, S.L., Lee, J.A., Fox, C.H., and Bao, Z. (2011). Skin-like pressure and strain sensors based on transparent elastic films of carbon nanotubes. *Nat. Nanotechnol.* 6, 788–792.
38. Kim, D.H., Lu, N., Ma, R., Kim, Y.S., Kim, R.H., Wang, S., Wu, J., Won, S.M., Tao, H., Islam, A., et al. (2011). Epidermal electronics. *Science* 333, 838–843.
39. Kaltenbrunner, M., Sekitani, T., Reeder, J., Yokota, T., Kuribara, K., Tokuhara, T., Drack, M., Schwodauer, R., Graz, I., Bauer-Gogonea, S., et al. (2013). An ultra-lightweight design for imperceptible plastic electronics. *Nature* 499, 458–463.
40. Yin, H., Cao, Y., Marelli, B., Zeng, X., Mason, A.J., and Cao, C. (2020). Soil sensors and plant wearables for smart and precision agriculture. *Adv. Mater.* 33. <https://doi.org/10.1002/adma.202007764>.
41. Tang, W., Yan, T., Ping, J., Wu, J., and Ying, Y. (2017). Rapid fabrication of flexible and stretchable strain sensor by chitosan-based water ink for plants growth monitoring. *Adv. Mater. Technol.* 2, 1700021.
42. Tang, W., Yan, T., Wang, F., Yang, J., Wu, J., Wang, J., Yue, T., and Li, Z. (2019). Rapid fabrication of wearable carbon nanotube/graphite strain sensor for real-time monitoring of plant growth. *Carbon* 147, 295–302.
43. Jiang, J., Zhang, S., Wang, B., Ding, H., and Wu, Z. (2020). Hydroprinted liquid-alloy-based morphing electronics for fast-growing/tender plants: from physiology monitoring to habit manipulation. *Small* 16, 2003833.
44. Kim, J.J., Allison, L.K., and Andrew, T.L. (2019). Vapor-printed polymer electrodes for long-term, on-demand health monitoring. *Sci. Adv.* 5, eaaw0463.
45. Nassar, J.M., Khan, S.M., Villalva, D.R., Nour, M.M., Almuslem, A.S., and Hussain, M.M. (2018). Compliant plant wearables for localized microclimate and plant growth monitoring. *NPJ Flex. Electron.* 2. <https://doi.org/10.1038/s41528-018-0039-8>.
46. Khan, S., Shaikh, S., Qaiser, N., and Hussain, M. (2018). Flexible lightweight cMOS-enabled multisensory platform for plant microclimate monitoring. *IEEE Trans. Electron Devices* 65, 5038–5044.

47. Zhao, Y., Gao, S., Zhu, J., Li, J., Xu, H., Xu, K., Cheng, H., and Huang, X. (2019). Multifunctional stretchable sensors for continuous monitoring of long-term leaf physiology and microclimate. *ACS Omega* 4, 9522–9530.
48. Lu, Y., Xu, K., Zhang, L., Deguchi, M., Shishido, H., Arie, T., Pan, R., Hayashi, A., Shen, L., Akita, S., and Takei, K. (2020). Multimodal plant healthcare flexible sensor system. *ACS Nano* 14, 10966–10975.
49. Im, H., Lee, S., Naqi, M., Lee, C., and Kim, S. (2018). Flexible Pi-based plant drought stress sensor for real-time monitoring system in smart farm. *Electronics* 7, 114.
50. Lan, L., Le, X., Dong, H., Xie, J., Ying, Y., and Ping, J. (2020). One-step and large-scale fabrication of flexible and wearable humidity sensor based on laser-induced graphene for real-time tracking of plant transpiration at bio-interface. *Biosens. Bioelectron.* 165, 112360.
51. Oren, S., Ceylan, H., Schnable, P.S., and Dong, L. (2017). High-resolution patterning and transferring of graphene-based nanomaterials onto tape toward roll-to-roll production of tape-based wearable sensors. *Adv. Mater. Technol.* 2, 1700223.
52. Zhao, F., He, J., Li, X., Bai, Y., Ying, Y., and Ping, J. (2020). Smart plant-wearable biosensor for in-situ pesticide analysis. *Biosens. Bioelectron.* 170, 112636.
53. Lee, K., Park, J., Lee, M.S., Kim, J., Hyun, B.G., Kang, D.J., Na, K., Lee, C.Y., Bien, F., and Park, J.U. (2014). In-situ synthesis of carbon nanotube-graphite electronic devices and their integrations onto surfaces of live plants and insects. *Nano Lett.* 14, 2647–2654.
54. Frazier, K.M., and Swager, T.M. (2013). Robust cyclohexanone selective chemiresistors based on single-walled carbon nanotubes. *Anal. Chem.* 85, 7154–7158.
55. Jaini, A.K.A., Hughes, L.B., Kitimet, M.M., Ulep, K.J., Leopold, M.C., and Parish, C.A. (2019). Halogen bonding interactions for aromatic and nonaromatic explosive detection. *ACS Sens.* 4, 389–397.
56. Kamyshny, A., and Magdassi, S. (2019). Conductive nanomaterials for 2D and 3D printed flexible electronics. *Chem. Soc. Rev.* 48, 1740.
57. Angione, M.D., Pilolli, R., Cotrone, S., Magliulo, M., Mallardi, A., Palazzo, G., Sabbatini, L., Fine, D., Dodabalapur, A., Cioffi, N., and Torsi, L. (2011). Carbon based materials for electronic bio-sensing. *Mater. Today* 14, 424–433.
58. Nekoueian, K., Amiri, M., Sillanpaa, M., Marken, F., Boukherroub, R., and Szunerits, S. (2019). Carbon-based quantum particles: an electroanalytical and biomedical perspective. *Chem. Soc. Rev.* 48, 4281–4316.
59. Yang, L., Yi, N., Zhu, J., Cheng, Z., Yin, X., Zhang, X., Zhu, H., and Cheng, H. (2020). Novel gas sensing platform based on a stretchable laser-induced graphene pattern with self-heating capabilities. *J. Mater. Chem. A* 8, 6487–6500.
60. An, N., Domel, A.G., Zhou, J., Rafsanjani, A., and Bertoldi, K. (2019). Programmable hierarchical kirigami. *Adv. Funct. Mater.* 30, 1906711.
61. Xue, Z., Song, H., Rogers, J.A., Zhang, Y., and Huang, Y. (2019). Mechanically-guided structural designs in stretchable inorganic electronics. *Adv. Mater.* 32, 1902254.
62. Cui, Z., Poblete, F.R., and Zhu, Y. (2019). Tailoring the temperature coefficient of resistance of silver nanowire nanocomposites and their application as stretchable temperature sensors. *ACS Appl. Mater. Interfaces* 11, 17836–17842.
63. Song, Z., Wang, X., Lv, C., An, Y., Liang, M., Ma, T., He, D., Zheng, Y.J., Huang, S.Q., Yu, H., and Jiang, H. (2015). Kirigami-based stretchable lithium-ion batteries. *Sci. Rep.* 5, 10988.
64. Tang, Y., and Yin, J. (2017). Design of cut unit geometry in hierarchical kirigami-based auxetic metamaterials for high stretchability and compressibility. *Extreme Mech. Lett.* 12, 77–85.
65. Xu, F., and Zhu, Y. (2012). Highly conductive and stretchable silver nanowire conductors. *Adv. Mater.* 24, 5117–5122.
66. Yao, S., Myers, A., Malhotra, A., Lin, F., Bozkurt, A., Muth, J.F., and Zhu, Y. (2017). A wearable hydration sensor with conformal nanowire electrodes. *Adv. Healthc. Mater.* 6, 1601159.
67. Yu, Z., Zhang, Q., Li, L., Chen, Q., Niu, X., Liu, J., and Pei, Q. (2011). Highly flexible silver nanowire electrodes for shape-memory polymer light-emitting diodes. *Adv. Mater.* 23, 664–668.
68. Lee, P., Lee, J., Lee, H., Yeo, J., Hong, S., Nam, K.H., Lee, D., Lee, S.S., and Ko, S.H. (2012). Highly stretchable and highly conductive metal electrode by very long metal nanowire percolation network. *Adv. Mater.* 24, 3326–3332.
69. Majchrzak, T., Wojnowski, W., Dymerski, T., Gebicki, J., and Namiensik, J. (2018). Electronic noses in classification and quality control of edible oils: a review. *Food Chem.* 246, 192–201.
70. Cipriano, D., and Capelli, L. (2019). Evolution of electronic noses from research objects to engineered environmental odour monitoring systems: a review of standardization approaches. *Biosensors* 9, 75.
71. Hu, W., Wan, L., Jian, Y., Ren, C., Jin, K., Su, X., Bai, X., Haick, H., Yao, M., and Wu, W. (2018). Electronic noses: from advanced materials to sensors aided with data processing. *Adv. Mater. Technol.* 4, 1800488.
72. Yang, T., Doherty, J., Guo, H., Zhao, B., Clark, J.M., Xing, B., Hou, R., and He, L. (2019). Real-time monitoring of pesticide translocation in tomato plants by surface-enhanced Raman spectroscopy. *Anal. Chem.* 91, 2093–2099.
73. Huang, C.B., Witomska, S., Aliprandi, A., Stoeckel, M.A., Bonini, M., Ciesielski, A., and Samori, P. (2019). Molecule-graphene hybrid materials with tunable mechanoresponse: highly sensitive pressure sensors for health monitoring. *Adv. Mater.* 31, e1804600.
74. Kang, M., Kim, J., Jang, B., Chae, Y., Kim, J.H., and Ahn, J.H. (2017). Graphene-based three-dimensional capacitive touch sensor for wearable electronics. *ACS Nano* 11, 7950–7957.
75. Korte, K.E., Skrabalak, S.E., and Xia, Y.N. (2008). Rapid synthesis of silver nanowires through a CuCl- or CuCl₂-mediated polyol process. *J. Mater. Chem.* 18, 437–441.
76. Frens, G. (1973). Controlled nucleation for the regulation of the particle size in monodisperse gold suspensions. *Nat. Phys. Sci.* 241, 20–22.